The Flow Pattern in an Industrial Paper Pulp Chest with a Side Entering Impeller

André Bakker
Julian B. Fasano
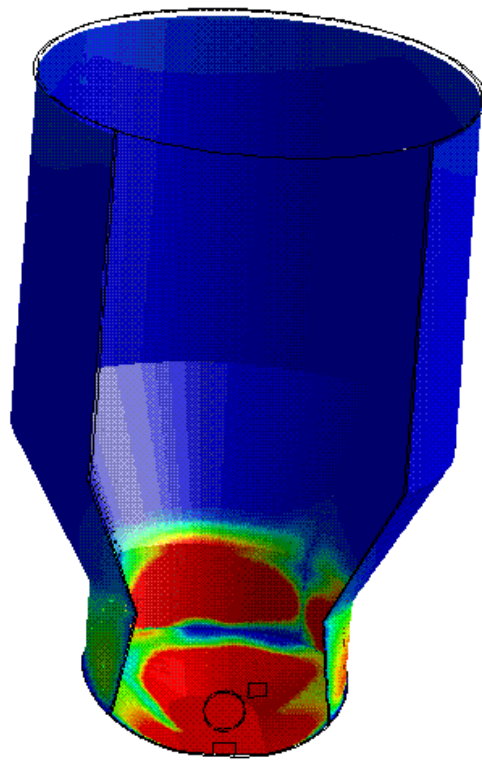
A mathematical model for the combined laminar and turbulent flow of paper pulp has been developed. The results of the model predictions agree well with experimental data.

   The model is used to analyze the flow pattern in an industrial paper pulp chest equipped with a side entering impeller. Turbulent, laminar and stagnant regions can easily be located. The model is an excellent tool for the optimization of agitators for large industrial paper pulp chests.

Updated: February 15, 2000

INTRODUCTION

Recently significant progress has been made in the application of Computational Fluid Dynamics (CFD) to the analysis of fluid flow in stirred chests. However, most work concentrated on the computation of flow patterns in lab-scale tanks equipped with top entering impellers.

Industrial problems are usually much harder to tackle. Complicating factors are the use of fluids with complex non-Newtonian behavior, the use of side entering agitators instead of top entering agitators and the fact that the agitator may be operated in the transitional regime.

Figure 1 *A typical shear stress vs. shear rate diagram for paper pulp.*

A difficult mixing problem is found in the paper industries. The paper pulp, which is a suspension of thin, flexible fibers, exhibits a very complex rheology. As a result of this rheology multiple flow regimes are found in paper pulp storage tanks. Part of the chest will be laminar; some parts of the chest are turbulent.

Pulp storage chests can be rectangular or cylindrical. The bottom of the chest is usually filleted, sloped and/or curved. Although paper pulp chests are sometimes equipped with top entering agitators, the paper industry prefers using side entering agitators.

The curved bottom shape and the side entering agitator require the use of body fitted grids for CFD modeling of this type of stirred tanks. The fact that multiple flow regimes occur makes modeling difficult since there are no well tested models for this type of flow available.

This paper deals with the development of a mathematical model for the flow of paper pulp in stirred tanks. First the model will be described. The model predictions will then be compared with experimental results for a lab-scale tank. Finally, the model will be used to predict the flow pattern in an industrial chest.

RHEOLOGICAL PROPERTIES OF FIBER SUSPENSIONS

The rheological properties of fiber suspensions are discussed by Gullichsen (1985). Figure 1 shows a typical shear stress vs shear rate diagram. This diagram shows that the fiber suspension initially behaves as a non-Newtonian fluid with a shear stress τ_y. When the shear stress exceeds a certain value τ_d the fiber network structure is disrupted and the suspension behaves nearly as a turbulent Newtonian fluid.

As a result of this rheological behavior fiber suspensions are extremely difficult to agitate. To provide motion through the whole tank the shear stress has to exceed the yield stress everywhere in the fluid. Since gradients in shear stresses can be expected, there will be regions in the fluid where the fiber network structure is disrupted and the flow will be turbulent. At the same time the flow may be laminar or even be stagnant in other parts of the chest.

This combination of turbulent flow and laminar flow of a non-Newtonian fluid makes this
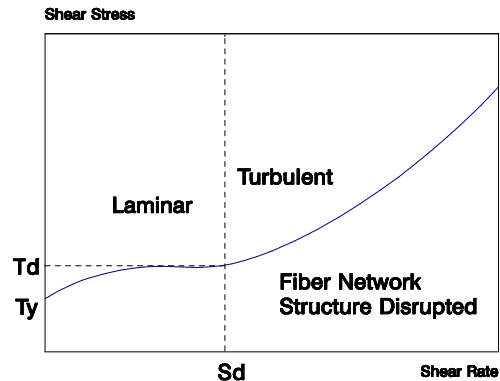
a difficult to model problem with CFD. As far as the present authors know, no other work has been published about the direct computation of this type of flow in stirred tanks.

DESCRIPTION PAPER PULP MODEL

The computational model is based on solving the conservation equations which describe the flow in the tank. For the mean flow of an incompressible liquid, the equation for the conservation of mass reads:

$$\frac{\partial U_i}{\partial x_i} = 0 \tag{1}$$

U_i denotes the mean velocity in direction x_i. Under steady-state laminar flow conditions the momentum balance is given by:

$$\rho U_j \frac{\partial U_i}{\partial x_j} = -\frac{\partial p}{\partial x_i} + \frac{\partial \tau_{ij}}{\partial x_j} + \rho g_i \tag{2}$$

The stress tensor τ_{ij} is given by:

$$\tau_{ij} = \mu \left(\frac{\partial U_i}{\partial x_j} + \frac{\partial U_j}{\partial x_i} \right) \tag{3}$$

When the flow is turbulent an additional term appears in the momentum balance for the mean flow:

$$\rho U_j \frac{\partial U_i}{\partial x_j} = -\frac{\partial p}{\partial x_i} + \frac{\partial}{\partial x_j}\left(\tau_{ij} + \rho \overline{u_i u_j} \right) + \rho g_i \tag{4}$$

u_i is the fluctuating, turbulent, velocity component in direction x_i. The cross correlation term $\overline{u_i u_j}$ denotes the Reynolds stress tensor. Although analytical equations for the Reynolds stress tensor can be derived, these equations again contain higher order cross correlation terms, and the set of equations is not closed. For modeling the Reynolds stresses various so-called turbulence models are available. An often used model is the k-ε model which models the Reynolds stresses as being proportional to gradients in the mean flow.

$$\rho \overline{u_i u_j} = -\mu_t \left(\frac{\partial U_i}{\partial x_j} + \frac{\partial U_j}{\partial x_i} \right) + \frac{2}{3} \delta_{ij} k \tag{5}$$

The turbulent viscosity μ_t is given by:

$$\mu_t = C_\mu \rho \frac{k^2}{\varepsilon} \tag{6}$$

The model equations for the conservation of the turbulent kinetic energy density k and the turbulent energy dissipation rate density ε are:

$$U_k \frac{\partial k}{\partial x_k} = \frac{\partial}{\partial x_k} \left([\nu + \nu_t / \sigma_k] \frac{\partial k}{\partial x_k} \right) + P_k - \varepsilon \tag{7}$$

$$U_k \frac{\partial \varepsilon}{\partial x_k} = \frac{\partial}{\partial x_k} \left([\nu + \nu_t / \sigma_\varepsilon] \frac{\partial \varepsilon}{\partial x_k} \right) + C_{\varepsilon 1} \frac{\varepsilon}{k} P_k - \varepsilon \tag{8}$$

Equation (5) for the Reynolds stresses is similar to equation (3) for the laminar shear stresses. The turbulent viscosity μ_t plays the same role as the molecular viscosity μ. As a result the form of the turbulent momentum equations is similar to the form of the laminar momentum equation except that μ is replaced by an effective viscosity μ_{eff}:

$$\mu_{eff} = \mu + \mu_t \tag{9}$$

For modeling the fiber suspension, which is partly laminar and partly turbulent, the following method was used. For every computational cell the computations are first performed as if the flow is turbulent. After that it is checked if the total shear stress is indeed larger than τ_d

$$(\mu + \mu_t) S \geq \tau_d \tag{10}$$

The shear rate S is calculated as the square root of the scalar invariant of the shear rate tensor:

$$S = \sqrt{\frac{\partial U_i}{\partial x_j} \left(\frac{\partial U_i}{\partial x_j} + \frac{\partial U_j}{\partial x_i} - \frac{2}{3} \delta_{ij} \frac{\partial U_l}{\partial x_l} \right)} \tag{11}$$

If equation (10) is not satisfied

$$(\mu + \mu_t)\, S \; < \; \tau_d \tag{12}$$

then the calculations for that particular cell are repeated as if the flow is laminar. The local apparent viscosity is then calculated from the experimental shear rate - shear stress curves and the local shear rate S.

The CFD solver used in this work is Fluent V4. Fluent contains the k-ε model for turbulent flow, but does not contain any models for combined laminar and turbulent flow. The additional equations were coded in Fortran subroutines and linked to the Fluent solver. The solver was then configured such that these additional subroutines were called every iteration.

EXPERIMENTAL VERIFICATION

Usually the results of CFD models are verified by performing flow visualizations, e.g. with the aid of Laser Doppler velocity measurements or other techniques, and comparing the results with the model predictions. Here this is not possible since it is not possible to see through the fiber suspension.

To allow for easier flow visualization a model fluid was designed. The model fluid consists of a suspension of glass fibers in a mixture of Tetrachloroethylene (TCE) and Carbondisulfide (CS_2). The concentrations of TCE and CS_2 were chosen such that the refractive index of the mixture matched the refractive index of the suspended glass fibers. The resulting mixture was clear enough to be able to see through and to spot the motion of tracer particles, despite a 10% volume holdup of glass fibers.

The experimental set up consisted of a cylindrical glass vessel with a diameter of 0.3 m
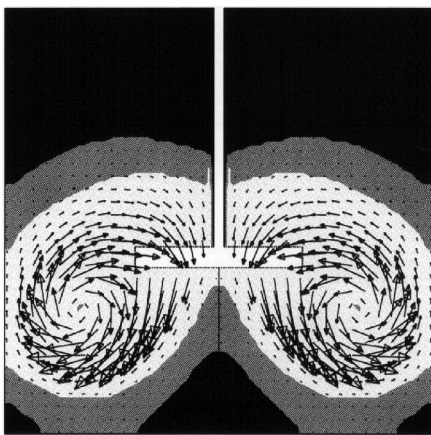
Figure 2 *Model predictions. black: stagnant; dark grey: laminar; light grey: turbulent.*
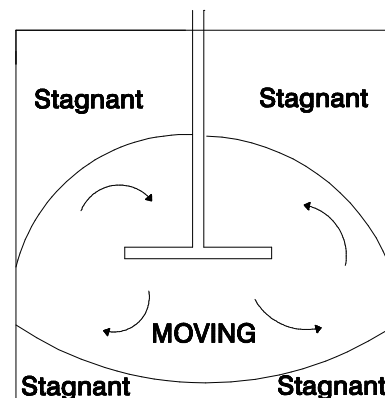
Experimental Visualization

Figure 3 *Experimental visualization.*

equipped with a 0.12 m Chemineer HE-3 impeller, operating at a speed of N = 10.8 1/s (= 650 RPM). The experiments were performed with a top entering impeller. The fact that the model will later be applied to tanks with side entering agitators is not expected to be a problem.

White tracer particles were added to the tank. A video film of the experiment was made and pictures were taken. The results of the flow visualization experiments were then compared with the results of the model calculations.

Figure 2 shows the model predictions for this tank. The model predicts three zones in the tank: turbulent flow, laminar flow and stagnant. The region around the impeller is characterized by high velocities and is turbulent. This is the only region where the shear stresses are large enough to disrupt the fiber network structure. Around this turbulent zone there is a zone where the fiber suspension is moving but where the stresses are not large enough to disrupt the fiber network and where the flow will be creeping laminar. Even further away from the impeller, in the corners at the bottom and in the top of the tank the suspension is not moving at all.

These predictions compare well with the experimental results. The experimental results are summarized in Figure 3. In the experiments it was not possible to distinguish between laminar and turbulent flow. The experiments show larger stagnant zones than the model predictions do. However, in most regions where the flow should be stagnant the model predicts very low velocities. The overall comparison between the model predictions and the experiments is satisfactory.

INDUSTRIAL CHESTS

A typical industrial paper pulp chest is shown in Figure 4. The sides of the chest are 10 m each and the liquid level is 7 m. The bottom of the chest is curved. The side entering impeller is mounted near the draining point. This is the generally accepted procedure in the paper industries.

The agitator studied here was a 1.22 m (= 48") diameter Chemineer HE-3S impeller running at 4.67 1/s (= 280 RPM). The computer model was used to study the flow pattern generated by this agitation system for various pulp consistencies. The consistency is defined as the mass fraction of bone dry paper fibers. The shear stress vs. shear rate curves used here were the curves published by Gullichsen for Softwood Kraft pulp. Other types of paper pulp have will have different rheological behavior depending on, amongst other things, fiber length and diameter.

The body fitted computational grid (see Figure 4) was generated with Fluent PreBFC V4 and then exported to Fluent V4 for the computations and the post processing. The tank was divided in 30x30x21 = 18,900 internal cells.

RESULTS

Figure 5 shows the predicted velocity vectors in a plane through the impeller for turbulent flow of water. The jet coming from the impeller impinges on the opposite chest wall and a long circulation loop is formed.
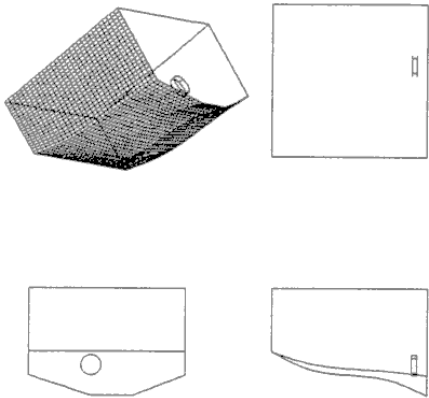
Figure 4 *Outline and grid.*
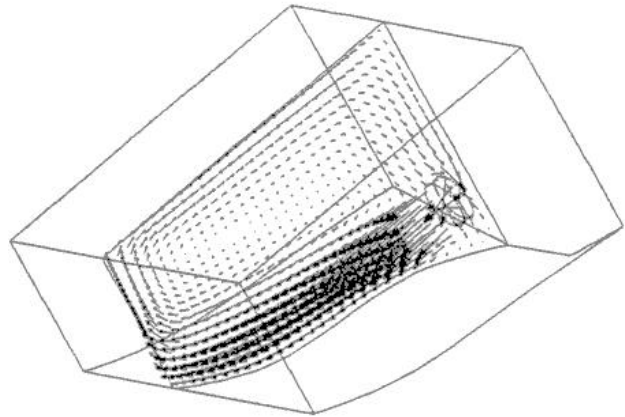
Figure 5 *Velocity vectors for water.*
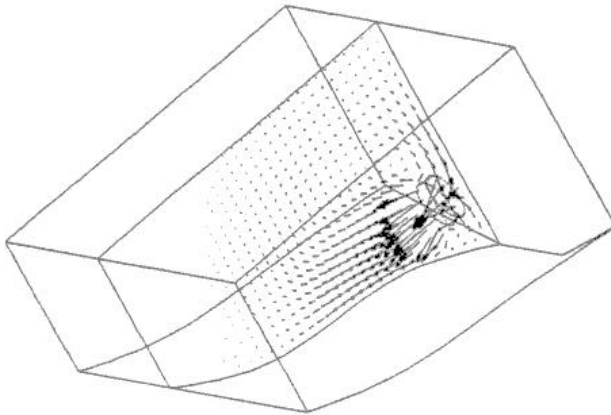
Figure 6 *Velocity vectors, 1% pulp.*
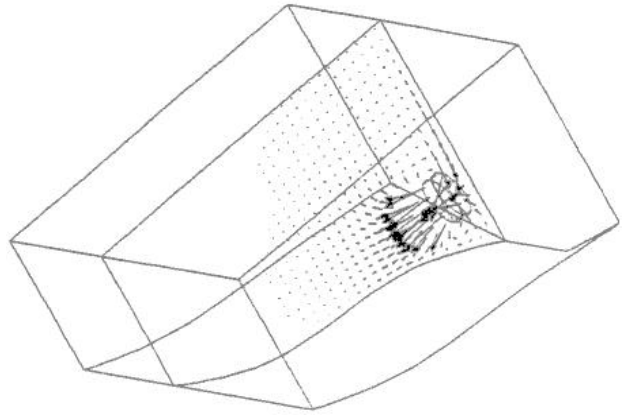
Figure 7 *Velocity vectors, 3.5% pulp.*
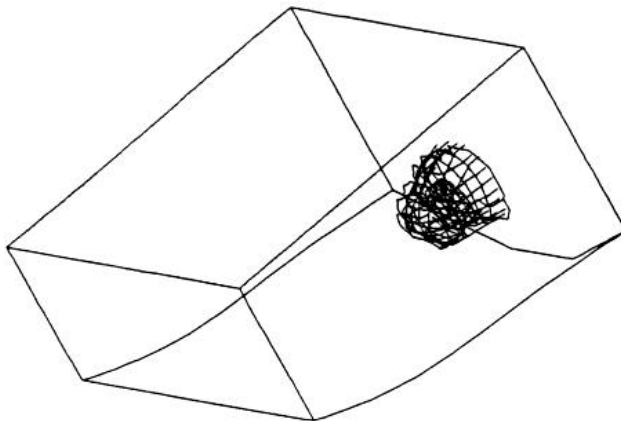
Figure 8 *Turbulent volume, 5% pulp.*
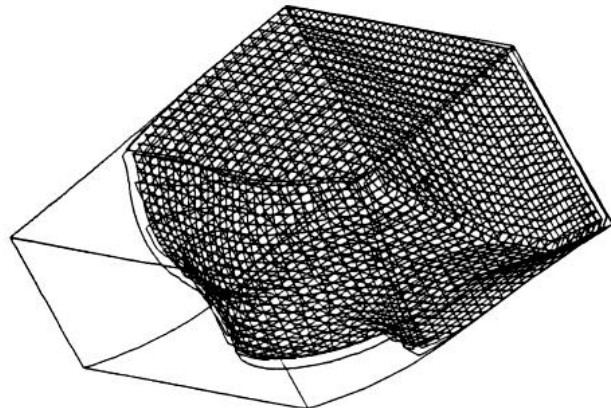
Figure 9 *Volume with velocities larger than 1E-3 m/s for 5% pulp.*

Figures 6 and 7 show the velocity vectors in the same plane for pulp consistencies from 1% and 3.5%. The size of the circulation loop decreases with increasing pulp consistency.

The length of the arrows is proportional to the local velocity. Short arrows denote low velocities; long arrows denote large velocities. No arrows at all means that the velocities are too small to be displayed, although they are not necessarily zero.

Figure 8 shows a wireframe surrounding the volume around the impeller where the shear stresses are large enough to disrupt the fiber network structure and where the flow will be turbulent (5% consistency). Figure 9 shows a similar wireframe, but

Figure 10 *Volume fraction as a function of minimum velocity (m/s).*

here the wireframe encloses the volume where the velocities are larger than 1E-3 m/s. The region outside the wireframe can be regarded as stagnant.

Figure 10 shows a velocity distribution diagram. The volume fraction of fluid moving with a velocity larger than a certain minimum velocity is plotted for various consistencies. This diagram shows that this agitator provides motion control for consistencies which are lower than 5%, which agrees well with the results of the Chemineer design procedures. The velocities of 1E-3 m/s may seem low at first, but creeping laminar flow is usually all that is needed in this type of storage chests.

CONCLUSIONS

For the first time a model has been developed for the multi-regime flow of a fluid with a complex rheology like paper pulp. The results of the model calculations agree satisfactory with experimental flow visualizations.

The model can be used to predict the flow pattern in large industrial chests where zones with turbulent mixing, zones with laminar mixing and stagnant zones can easily be located. This model is an excellent tool for the optimization of agitators for large industrial chests.

REFERENCES

[1]   Gullichsen J. (1985)
         Medium Consistency Processing - Fundamentals
         Bleach Plant Operations/TAPPI Seminar Notes, 135-142

NOTATION

$c_{\varepsilon 1}$	Model Constant	(-)
$c_{\varepsilon 2}$	Model Constant	(-)
g	Acceleration by Gravity	$(m\ s^{-2})$
k	Turbulent Kinetic Energy Density	$(m^2 s^{-2})$
N	Impeller Rotational Speed	(s^{-1})
p	Pressure	(Pa)
P_k	Production of k	$(m^2 s^{-3})$
S	Shear Rate	(s^{-1})
u	Fluctuating Component of Velocity	$(m\ s^{-1})$
U	Mean Velocity	$(m\ s^{-1})$
x	Coordinate	(m)
ρ	Density of Fluid	$(kg\ m^{-3})$
δ	Dirac Delta function	(-)
σ_e	Model Constant	(-)
σ_k	Model Constant	(-)
τ	Shear Stress	(Pa)
τ_d	Disruptive Shear Stress	(Pa)
τ_y	Yield Stress	(Pa)
μ	Molecular Viscosity	$(Pa\ s)$
μ_t	Turbulent Viscosity	$(Pa\ s)$
μ_{eff}	Effective Viscosity	$(Pa\ s)$
ν	μ/ρ	$(m\ s^{-2})$
ν_t	μ_t/ρ	$(m\ s^{-2})$